Title

Ca^{2+}-driven cytoplasmic backflow secures spindle position in fertilized mouse eggs

Authors

Takaya Totsuka[1,2,3] and Miho Ohsugi[1,2] *

Affiliations

1. Department of Life Sciences, Graduate School of Arts and Sciences, The University of Tokyo, Komaba 3-8-1, Meguro-ku, Tokyo 153-8902, Japan.
2. Department of Life Sciences, Graduate School of Arts and Sciences, The University of Tokyo, Hongo, Bunkyo-ku, Tokyo, 113-0033, Japan.
3. Cell and Developmental Biology Center, National Heart, Lung, and Blood Institute, National Institutes of Health, Bethesda 20892, MD, USA.

Contact info

*Correspondence: mihoohsugi@g.ecc.u-tokyo.ac.jp

Abstract

Fertilization triggers hours-long Ca^{2+} oscillations in mammalian eggs, but the effects of repeated Ca^{2+} surges remain unclear. Here, we investigate spindle dynamics and its relationship with cytoplasmic streaming in fertilized mouse eggs. The spindle, initially parallel to the plasma membrane, rotates vertically, in accordance with previously reported results using artificially activated eggs. Intriguingly, it transiently reverses its rotation direction in synchrony with Ca^{2+} oscillations, regardless of artificially altered frequency. This effect results from cytoplasmic streaming, initially moving from spindle to egg center, displaying a Ca^{2+}-dependent backflow. Streaming also impacts spindle positioning, balancing spindle rotation and cortical localization maintenance. We provide evidence that Ca^{2+}-dependent cortical myosin II activation causes actomyosin contraction, leading to transient streaming towards non-contracting actin cap regions overlaying chromosomes. Our findings underscore the role of Ca^{2+} oscillations in maintaining spindle position in fertilized eggs, thereby ensuring highly asymmetric division and preservation of maternal stores in zygotes.

Main

In vertebrates, eggs are arrested at metaphase II (Meta-II) while awaiting fertilization. The fusion between sperm and egg induces an elevation in free cytoplasmic Ca^{2+}, triggering release from Meta-II arrest and the onset of Anaphase II (Ana-II)[1–4]. Consequently, one set of segregated chromosomes is extruded into a smaller cell, known as the second polar body (PB2). The other set of chromosomes in the larger cell contribute to development together with the sperm-derived chromosomes[5]. This process is conserved among vertebrates. However, mammals exhibit unique features, such as the delay in pronuclear (PN) formation that takes over an hour following chromosome segregation[6–10]. Furthermore, in mouse Ana-II eggs, the spindle, initially parallel to the plasma membrane, must rotate perpendicularly[5,11,12]. In parthenogenetically activated eggs, the inward cytoplasmic streaming, generated in an actomyosin dependent manner, aids in rotating the Ana-II spindle. However, it remains unknown how the Ana-II spindle rotates in fertilized eggs while retaining its cortical localization, resisting the inward streaming.

Most non-mammalian species present a single or few waves of Ca^{2+} transients after fertilization, while mammals exhibit repeated Ca^{2+} oscillations over several hours until pronuclear formation[13]. However, the initial Ca^{2+} transient triggers primarily egg activation events, including meiotic resumption and polyspermy blocking[14–18] and the biological importance of continued Ca^{2+} oscillations during the long Ana-II remains unclear.

In this article, we address these issues by developing a live-imaging method for mouse in vitro fertilized (IVF) eggs. Our findings indicate that each Ca^{2+} oscillation induces cortical actomyosin contraction, generating transient cytoplasmic backflow. This repetitive inversion of cytoplasmic streaming helps maintain the subcortical localization of the rotating Ana-II spindle, propelling it back to the cortex when displaced. Our results highlight the importance of mammalian-specific Ca^{2+} oscillations in retaining spindle position to form a small polar body and a large egg, preserving maternal stores.

Results

Rotating Ana-II spindle in IVF eggs shows periodic, transient decrease in rotation angle

To investigate spindle rotational movement within fertilized mouse eggs, we first established a method for live imaging of the spindle dynamics throughout the process of IVF. We prepared a glass-bottom dish with two nearby medium drops, one with a Meta-II egg expressing EGFP-tagged α-tubulin and mRFP1-tagged histone H2B, and the other with sperm, all covered with liquid paraffin. Before placing the eggs in the medium drop, an opening in the zona pellucida for sperm entry was made. The egg was positioned in the medium drop so that the long axis of the Meta-II spindle aligned parallel to the focal plane at the equatorial plane of the egg, and then stabilized using a holding pipette. After initiating live observation, two drops of medium were

connected for insemination (Fig. 1a). Confocal images, covering the entire short axis of the Meta-II spindle, were collected every 1 μm along the z-axis for a total depth of 15 μm. Using this imaging protocol, we captured the dynamics of the chromosomes and spindles from Meta-II to the extrusion of PB2 continuously (Fig. 1b and supplementary Video 1). This indicates that chromosome segregation and spindle rotation occurred in the xy-plane, where the long axis of the Meta-II spindle lies, with minor movement along the z-axis. This allowed us to analyze spindle dynamics in detail using z-stack projection images.

The rotational movement of the Ana-II spindle was analyzed using time-lapse images taken every minute. In each image, the midpoint of the centroids of the separated chromosomes was defined as the spindle midpoint; and the angle formed by the line connecting the chromosome centroids and the line connecting the spindle midpoint and the centroid of the egg cell was defined as the angle (α) (Fig. 1c). We set the angle (α) in the image taken 10 min after the onset of Ana-II (α_{10}) as the standard and plotted subsequent changes in angle as the spindle rotation angle (α_{sp}). Overall, the spindle angle increased over time, aligning with previously reported results using parthenogenetically activated eggs[19,20]. However, most IVF eggs exhibited a periodic, transient decrease in the rotation angle (Fig. 1d).

Ca^{2+} oscillations cause repeated transient inversions in the direction of spindle rotation

A decrease in the rotation angle was observed every 5–15 min, although the interval varied among eggs. This pattern is similar to the interval between transient increases in Ca^{2+} in fertilized mouse eggs[21]. As expected, simultaneous observation of spindle dynamics and intracellular Ca^{2+} changes in IVF eggs revealed that when the Ca^{2+} concentration was low, spindles rotated in a positive direction; however, immediately after a Ca^{2+} transient, the direction of spindle rotation changed rapidly and temporarily switched to a negative direction (Fig. 2a,b and expanded Fig. 1a and Supplementary Video 2, top panels). A correlation between the temporal reversal of the rotational direction of the spindle and the Ca^{2+} transient was also observed in eggs activated by Sr^{2+} (hereafter referred to as Sr^{2+}-activated eggs), which exhibit Ca^{2+} oscillations similar to fertilized eggs[22] (Fig. 2c,d and Expanded Data Fig. 1b and Supplementary Video 2, bottom panels). These results demonstrate that the periodicity of spindle rotational movement coincides with that of Ca^{2+} oscillations independent of sperm-derived factors.

Next, to examine the impact of changes in Ca^{2+} oscillations on the spindle rotation, we first tried to increase the frequency of Ca^{2+} oscillations using human-PLCζ[23–25]. Exogenously expressed human-PLCζ increased the frequency of Ca^{2+} oscillations in a dose-dependent manner, but only either before or after spindle rotation. We then combined human-PLCζ expression with Sr^{2+} activation and succeeded in triggering high-frequency Ca^{2+} oscillations during spindle rotation (Fig. 3a,b) . A correlation between the temporal change in the rotation direction and the

Ca^{2+} transient was observed even in eggs with increased frequency of Ca^{2+} oscillations (Fig 3b,c and Extended Data Fig. 1c). Second, thapsigargin, an inhibitor of sacro-ER Ca^{2+}-ATPase (SERCA)[26,27], was added to the medium during the early Ana-II to inhibit Ca^{2+} oscillations (Fig. 3d). Following this inhibition, the spindle exhibited smooth rotational movement, without any transient reversal in its rotation direction (Fig. 3e and Extended Data Fig. 1d). Together, these results indicate that elevated cytoplasmic Ca^{2+} levels reverse spindle rotation.

Ca^{2+}-induced outward cytoplasmic streaming causes a reversal of spindle rotation

To further investigate the Ca^{2+}-dependent changes in the direction of spindle rotation, we analyzed cytoplasmic streaming, considering its supposed role in driving spindle rotation during Ana-II[19,20]. Using particle image velocimetry (PIV; see Materials and Methods), we revealed that in Ana-II, inward cytoplasmic streaming was observed as previously reported[19], but immediately after the Ca^{2+} levels peaked, the orientation of the streaming reversed transiently to outward (Fig. 4a-c and Expanded Data Fig. 2a and Supplementary Video 3). The directions of spindle rotation and cytoplasmic streaming always coincided: when cytoplasmic streaming was inward or outward, the spindle rotated in the positive or negative direction, respectively (Expanded Data Fig. 2b). To clarify the causal relationship between directional changes of cytoplasmic streaming and spindle rotation, we utilized a method of partial spindle disruption using low-dose nocodazole. This approach halted chromosome segregation and spindle rotation without compromising meiotic resumption upon egg activation[28]. The low-dose nocodazole did not affect Ca^{2+} oscillations, and the cytoplasmic streaming was oriented outward immediately after each Ca^{2+} transient, even in the absence of spindle rotation (Fig. 4d-f and Expanded Data Fig. 2c and Supplementary Video 4). These results demonstrate that elevated cytoplasmic levels of Ca^{2+} induce the inversion of cytoplasmic streaming, thereby changing the direction of spindle rotation.

Ca^{2+} oscillations are involved in the maintenance of the subcortical localization of the Ana-II spindle and ensure the extrusion of small-sized PB2

What is the physiological importance of Ca^{2+}-induced changes in cytoplasmic streaming? To address this question, we next focused on the position of the Ana-II spindle because in Meta-II-arrested eggs, both inward and outward cytoplasmic streaming affect the position of the spindle and even transports it to the egg center[29]. The position of the Ana-II spindle was analyzed by measuring the distance between the midpoint of the spindle and the centroid of the egg (Fig. 5a). In most of the Sr^{2+}-activated eggs, inward cytoplasmic streaming resulted in a slight displacement of the spindle toward the interior of the egg. Conversely, when outward cytoplasmic streaming occurred, the spindle relocated toward the cortex, while consistently maintaining a certain distance from the plasma membrane (Fig. 5b,c). We also observed an egg in which the spindle

unintentionally shifted away from the cell membrane during the early Ana-II stage. In this egg, the spindle gradually moved closer to the plasma membrane each time the cytoplasm flowed outward (Fig. 5d,e). These results suggest that transient, repetitive outward cytoplasmic streaming induced by Ca^{2+} oscillations is involved in maintaining the subcortical localization of the Ana-II spindle.

Subcortical localization of the Ana-II spindle is essential for the formation of the small PB2[30]. Therefore, to examine this hypothesis, we tested the effect of no- or lower-frequency of Ca^{2+} oscillations on the size of the PB2. First, we activated eggs with Sr^{2+} or 7% ethanol and found that 9.1% and 18.6% of the eggs, respectively, extruded a larger PB2 (Fig. 5f,g). Additionally, Sr^{2+}-activated eggs were treated with thapsigargin 10 min after immersing them in the Sr^{2+}-containing medium drop. This inhibited Ca^{2+} oscillations almost completely before the beginning of spindle rotation (Supplementary Video 5). In the presence of 5 or 10 μM thapsigargin 11.1% and 13.4% of eggs extruded a large-sized PB2, respectively, whereas 7.7% of the control DMSO-treated activated eggs formed a larger PB2 (Fig. 5f,g). These results suggest that Ca^{2+} oscillations change the direction of cytoplasmic streaming toward the chromosomes, thereby contributing to the maintenance of the subcortical localization of the rotating spindle (Fig. 5h).

Cortical actomyosin contraction generates cytoplasmic flow toward the non-contracted actin cap regions

To uncover the mechanisms underlying the change in cytoplasmic streaming upon elevated cytoplasmic Ca^{2+}, we first performed PIV analysis using time-lapse images of the IVF eggs, in which both maternal and paternal chromosomes appear within the same 15 μm thick z-sections. Similar to Sr^{2+}-activated eggs, the direction of cytoplasmic streaming in IVF eggs was inward from the regions of the Ana-II spindle during the intervals between each Ca^{2+} peak. In contrast, immediately after Ca^{2+} levels peaked, cytoplasmic streaming was oriented toward both the maternal and paternal chromosomes (Fig. 6 and Expanded Data Fig. 3 and Supplementary Video 6). These results suggest that elevated levels of cytoplasmic Ca^{2+} change the direction of cytoplasmic streaming toward the chromosomes, rather than simply backward.

Given that the contraction of actomyosin has been reported to drive cytoplasmic movement in fertilized eggs[31], we next proceeded with experiments to inhibit myosin II by adding blebbistatin 10 min after the onset of Ana-II. Ca^{2+} oscillations remained unaffected, yet the velocity of both inward and outward cytoplasmic streaming significantly decreased (Fig. 7a,b and Expanded Data Fig. 4 and Supplementary Video 7). This suggests that the activity of myosin II at disparate sites is the underlying cause of both inward and Ca^{2+}-dependent outward cytoplasmic streaming. To further examine this possibility, we visualized F-actin in Sr^{2+}-activated eggs and observed

178 periodic fluctuations in F-actin intensity (Supplementary Video 8). Quantitative analysis revealed
179 that in the cortical regions, the F-actin intensity increased concomitantly with a slight but distinct
180 contraction of the cortical plasma membrane, outward movement of cytoplasmic streaming, and
181 expansion of the protrusions in the actin cap regions (Fig. 7c-e). The changes in F-actin intensity
182 within the cytoplasm contrasted and complemented the changes in the cortical regions (Fig. 7e).
183 Previous studies demonstrate that active myosin II was localized exclusively to the regions
184 surrounding the two protrusions overlying the segregated chromosomes and the furrow region
185 enclosed by these two protrusions, as well as to the region surrounding the fertilization
186 cone[19,20,31,32]. Immunofluorescence staining with an anti-phosphorylated regulatory myosin light
187 chain (pMLC) antibody revealed that in addition to these sites, approximately 12.4% of the Sr^{2+}-
188 activated eggs exhibited cortical MLC phosphorylation (Fig. 7f and Extended Data Fig. 5a,b),
189 whereas ethanol-activated eggs did not exhibit MLC phosphorylation at the cortex (Extended
190 Data Fig. 5c). Moreover, in Ana-II eggs with cortical MLC phosphorylation, cortical F-actin was
191 more pronounced than in those without cortical MLC phosphorylation (Fig. 7g), supporting the
192 idea that cortical actomyosin contraction causes cortical actin thickening.
193 In summary, we propose that Ca^{2+}-induced contraction of cortical actomyosin pushes the
194 adjacent cytoplasm toward the center of the cell. This merges into the streaming toward the
195 uncontracted regions, specifically the actin cap around the maternal chromosomes and the
196 fertilization cone around the paternal chromatin (Fig. 7h).
197
198 **Discussion**
199 In this study, we describe a first-time detailed examination of spindle dynamics in fertilized
200 mouse eggs. Our straightforward yet effective live imaging approach revealed two features of the
201 Ana-II spindle rotational movement in fertilized mouse eggs. First, the spindle rotates two-
202 dimensionally in the equatorial plane, wherein its long axis resides within the Meta-II egg. This
203 has been assumed in previous studies using artificially activated eggs but was directly
204 demonstrated in this study and could provide important insights into understanding the nature of
205 forces driving spindle rotation in mouse Ana-II eggs. Second, the rotating Ana-II spindle
206 transiently reverses its rotation direction upon cytoplasmic Ca^{2+} elevation. Repeated transient
207 changes in the rotation angle disappeared when Ca^{2+} oscillations were suppressed by thapsigargin
208 (Fig. 3e). This is consistent with previous reports that in ethanol-stimulated eggs, in which only a
209 single or a few waves of Ca^{2+} transients were observed, the rotation angle of the spindle increased
210 smoothly and with an almost constant velocity[19].
211 We have uncovered, for the first time, the effects induced in eggs by mammalian-specific
212 calcium dynamics, Ca^{2+} oscillations, triggered by sperm fusion. Our results show that throughout
213 Ana-II, the spindle undergoes a cycle wherein it is subjected to inward cytoplasmic streaming,

lasting several to tens of minutes, followed by a backflow of a few minutes that occurs in synchronization with Ca^{2+} oscillations. In Meta-II eggs, inhibition of the Arp2/3 complex induces myosin II-dependent inward cytoplasmic streaming, moving the spindle toward the egg center[29]. This implies that Ana-II spindle is constantly at risk of moving away from the cortex. Indeed, despite the centralspindlin complex anchoring the central spindle to the cortex[20], there are occasional instances where the spindle inadvertently detaches from the cortex (Fig. 5d,e and Supplementary Video 5, bottom panels). In such cases, Ca^{2+}-dependent cytoplasmic streaming toward the spindle counteracts the inward streaming and assists in maintaining cortical spindle localization. Thus, Ca^{2+} oscillations specific to mammalian eggs help mitigate the risks posed by the long-lasting Ana-II phase unique to mammals[8,10]. The Ana-II spindle rotation is essential for the proper extrusion of PB2 in mouse eggs[5,12,33]. However, in many other mammals, including humans, the long axis of the Meta-II spindle is perpendicular to the cell membrane and does not require rotation[34–36]. In contrast, regardless of the spindle orientation, the Ana-II spindle must sustain its cortical localization until the completion of cytokinesis. Therefore, we believe that the importance of Ca^{2+}-dependent outward cytoplasmic streaming lies not in its ability to control spindle rotation speed, but in ensuring the subcortical localization of the Ana-II spindle and formation of a large fertilized egg[30].

Observation of fertilized eggs revealed that the Ca^{2+}-induced cytoplasmic streaming is not simply reversing the preceding flow, but is rather directed toward the membrane regions lined by the actin cap structure (Fig. 6 and Extended Data Fig. 3). Based on our results and previous observations[19,20], we propose that inward and outward cytoplasmic streaming is driven by the continuous contraction of actomyosin near the Ana-II spindle and intermittent contractions of other cortical membrane regions due to MLC phosphorylation by myosin light chain kinase (MLCK), which is activated by Ca^{2+}/CaM[14], respectively. This model can explain the distinctive changes in Ca^{2+}-dependent cytoplasmic streaming, which initially flows toward the developing PB2 as well as fertilization cone, would later transition into a fast, clear flow toward the fertilization cone after the formation of PB2[31,37].

Cytoplasmic movement in fertilized eggs can predict subsequent developmental potential[31]. This could be attributed to the effect of Ca^{2+}-independent and dependent cytoplasmic streaming on the arrangement of spindles, chromosomes, and various other organelles within the fertilized egg[38,39]. Observing the movement of cytoplasm and its impacts in zygotes of diverse mammals could further deepen our understanding of the significance of Ca^{2+} oscillations in mammals.

Main references

1. Jones, K. T. Mammalian egg activation: From Ca^{2+} spiking to cell cycle progression. *Reproduction* **130**, 813–823 (2005).
2. Rauh, N. R., Schmidt, A., Bormann, J., Nigg, E. A. & Mayer, T. U. Calcium triggers exit from meiosis II by targeting the APC/C inhibitor XErp1 for degradation. *Nature* **437**, 1048–1052 (2005).
3. Schmidt, A. *et al.* Xenopus polo-like kinase Plx1 regulates XErp1, a novel inhibitor of APC/C activity. *Genes Dev.* **19**, 502–513 (2005).
4. Schmidt, A., Rauh, N. R., Nigg, E. A. & Mayer, T. U. Cytostatic factor: An activity that puts the cell cycle on hold. *J. Cell Sci.* **119**, 1213–1218 (2006).
5. Maro, B., Johnson, M. H., Webb, M. & Flach, G. Mechanism of polar body formation in the mouse oocyte: An interaction between the chromosomes, the cytoskeleton and the plasma membrane. *J. Embryol. Exp. Morphol.* **VOL. 92**, 11–32 (1986).
6. Fan, H.-Y. & Sun, Q.-Y. Involvement of mitogen-activated protein kinase cascade during oocyte maturation and fertilization in mammals. *Biol. Reprod.* **70**, 535–547 (2004).
7. Soeda, S., Yamada, K. & Ohsugi, M. Inactivation of mitogen-activated protein kinase is neither necessary nor sufficient for the onset of pronuclear formation in mouse oocytes. *Genes to Cells* **18**, 850–858 (2013).
8. Soeda, S., Yamada-Nomoto, K., Michiue, T. & Ohsugi, M. RSK-MASTL Pathway Delays Meiotic Exit in Mouse Zygotes to Ensure Paternal Chromosome Stability. *Dev. Cell* **47**, 363-376.e5 (2018).
9. Tatemoto, H. & Muto, N. Mitogen-activated protein kinase regulates normal transition from metaphase to interphase following parthenogenetic activation in porcine oocytes. *Zygote* **9**, 15–23 (2001).
10. Zhou, C. & Homer, H. A. The oocyte spindle midzone pauses Cdk1 inactivation during fertilization to enable male pronuclear formation and embryo development. *Cell Rep.* **39**, 110789 (2022).
11. Maro, B. & Verlhac, M. H. Polar body formation: New rules for asymmetric divisions. *Nat. Cell Biol.* **4**, 281–283 (2002).
12. Wang, Q., Racowsky, C. & Deng, M. Mechanism of the chromosome-induced polar body extrusion in mouse eggs. *Cell Div.* **6**, 1–9 (2011).
13. Jones, K. T., Carroll, J., Merriman, J. A., Whittingham, D. G. & Kono, T. Repetitive sperm-induced Ca2+ transients in mouse oocytes are cell cycle dependent. *Development* **121**, 3259–3266 (1995).
14. Ducibella, T. & Fissore, R. The roles of Ca^{2+}, downstream protein kinases, and

oscillatory signaling in regulating fertilization and the activation of development. *Dev. Biol.* **315**, 257–279 (2008).

15. Ducibella, T., Kurasawa, S., Duffy, P., Kopf, G. S. & Schultz, R. M. Regulation of the polyspermy block in the mouse egg: Maturation-dependent differences in cortical granule exocytosis and zona pellucida modifications induced by inositol 1,4,5-trisphosphate and an activator of protein kinase C. *Biol. Reprod.* **48**, 1251–1257 (1993).
16. Ozil, J. P. *et al.* Egg activation events are regulated by the duration of a sustained [Ca^{2+}]cyt signal in the mouse. *Dev. Biol.* **282**, 39–54 (2005).
17. Schultz, R. M. & Kopf, G. S. 2 Molecular Basis of Mammalian Egg Activation. in (eds. Pedersen, R. A. & Schatten, G. P. B. T.-C. T. in D. B.) **30**, 21–62 (Academic Press, 1995).
18. Swann, K. & Ozil, J. P. Dynamics of the Calcium Signal That Triggers Mammalian Egg Activation. *Int. Rev. Cytol.* **152**, 183–222 (1994).
19. Dehapiot, B. *et al.* RhoA- And Cdc42-induced antagonistic forces underlie symmetry breaking and spindle rotation in mouse oocytes. *PLoS Biol.* **19**, 1–30 (2021).
20. Wang, H. Y. *et al.* Symmetry breaking in hydrodynamic forces drives meiotic spindle rotation in mammalian oocytes. *Sci. Adv.* **6**, (2020).
21. Swann, K., Saunders, C. M., Rogers, N. T. & Lai, F. A. PLCζ(zeta): A sperm protein that triggers Ca^{2+} oscillations and egg activation in mammals. *Semin. Cell Dev. Biol.* **17**, 264–273 (2006).
22. Zhang, D. *et al.* Strontium promotes calcium oscillations in mouse meiotic oocytes and early embryos through InsP3 receptors, and requires activation of phospholipase and the synergistic action of InsP3. *Hum. Reprod.* **20**, 3053–3061 (2005).
23. Miura, K. *et al.* Application of auxin-inducible degron technology to mouse oocyte activation with PLCζ. *J. Reprod. Dev.* **64**, 319–326 (2018).
24. Sato, K. *et al.* Molecular characteristics of horse phospholipase C zeta (PLCζ). *Anim. Sci. J.* **84**, 359–368 (2013).
25. Ito, M. *et al.* Difference in Ca^{2+} oscillation-inducing activity and nuclear translocation ability of PLCZ1, an egg-activating sperm factor candidate, between mouse, rat, human, and medaka fish. *Biol. Reprod.* **78**, 1081–1090 (2008).
26. Kline, D. & Kline, J. T. Thapsigargin activates a calcium influx pathway in the unfertilized mouse egg and suppresses repetitive calcium transients in the fertilized egg. *J. Biol. Chem.* **267**, 17624–17630 (1992).
27. Wakai, T., Zhang, N., Vangheluwe, P. & Fissore, R. A. Regulation of endoplasmic reticulum Ca^{2+} oscillations in mammalian eggs. *J. Cell Sci.* **126**, 5714–5724 (2013).
28. Totsuka, T. & Ohsugi, M. Production of mouse androgenetic embryos using spindle

perturbation. *Sci. Rep.* **10**, 1–9 (2020).

29. Yi, K. *et al.* Dynamic maintenance of asymmetric meiotic spindle position through Arp2/3-complex-driven cytoplasmic streaming in mouse oocytes. *Nat. Cell Biol.* **13**, 1252–1258 (2011).
30. Sun, S. C. *et al.* Arp2/3 complex regulates asymmetric division and cytokinesis in mouse oocytes. *PLoS One* **6**, (2011).
31. Ajduk, A. *et al.* Rhythmic actomyosin-driven contractions induced by sperm entry predict mammalian embryo viability. *Nat. Commun.* **2**, (2011).
32. Simerly, C., Nowak, G., De Lanerolle, P. & Schatten, G. Differential expression and functions of cortical myosin IIa and IIb isotypes during meiotic maturation, fertilization, and mitosis in mouse oocytes and embryos. *Mol. Biol. Cell* **9**, 2509–2525 (1998).
33. Zhu, Z.-Y. *et al.* Rotation of Meiotic Spindle Is Controlled by Microfilaments in Mouse Oocytes1. *Biol. Reprod.* **68**, 943–946 (2003).
34. Roeles, J. & Tsiavaliaris, G. Actin-microtubule interplay coordinates spindle assembly in human oocytes. *Nat. Commun.* **10**, 1–10 (2019).
35. Tremoleda, J. L., Schoevers, E. J., Stout, T. A., Colenbrander, B. & Bevers, M. M. Organisation of the cytoskeleton during in vitro maturation of horse oocytes. *Mol. Reprod. Dev.* **60**, 260–269 (2001).
36. Da Broi, M. G., Malvezzi, H., Paz, C. C. P., Ferriani, R. A. & Navarro, P. A. A. S. Follicular fluid from infertile women with mild endometriosis may compromise the meiotic spindles of bovine metaphase II oocytes. *Hum. Reprod.* **29**, 315–323 (2014).
37. Deguchi, R., Shirakawa, H., Oda, S., Mohri, T. & Miyazaki, S. Spatiotemporal analysis of Ca^{2+} waves in relation to the sperm entry site and animal-vegetal axis during Ca^{2+} oscillations in fertilized mouse eggs. *Dev. Biol.* **218**, 299–313 (2000).
38. Lu, W. & Gelfand, V. I. Go with the flow - bulk transport by molecular motors. *J. Cell Sci.* **136**, (2023).
39. Mori, M. *et al.* RanGTP and the actin cytoskeleton keep paternal and maternal chromosomes apart during fertilization. *J. Cell Biol.* **220**, (2021).

Figure legends

Fig.1 Spindle dynamics in IVF eggs

a, Schematics showing live imaging method for IVF eggs. Confocal images of z-slices covering the entire width of the spindle short axis in orientation-adjusted Meta-II eggs (left). Two medium drops, one containing a Meta-II egg held by a pipette and the other with sperm, were prepared on a paraffin-covered glass-bottom dish (middle). Two drops of medium were connected for insemination (right panel). **b,** Representative time-lapse images showing chromosomal and spindle dynamics in IVF eggs expressing mRFP1-tagged histone H2B (magenta) and EGFP-tagged-α-tubulin (green). The numbers above the top panels indicate the time before and after the onset of Ana-II. **c,** Schematics showing the quantification of the spindle rotation angle. **d,** Change over time in spindle rotation angle for six IVF eggs.

Fig.2 Direction of the spindle rotation transiently reverses coincidence with the Ca^{2+} transient

a,c, Graphs showing the spindle rotation angle (magenta) and relative intensity of cytoplasmic Ca^{2+} levels (green) in representative IVF **a**, or Sr^{2+}-activated **c** eggs. **b,d,** Heat maps showing the normalized angular velocity (Δt = 1 min) of spindle rotation for several minutes before and after the Ca^{2+} transient in IVF eggs (23 peaks, 8 IVF eggs) **b**, or in Sr^{2+}-activated eggs (34 peaks, 11 eggs) **d**. The timing of the Ca^{2+} transient is enclosed by a black square.

Fig.3 Inversions in the direction of spindle rotation depends on Ca^{2+} transients

a, The frequency of Ca^{2+} oscillations during 10 to 70 min after Ana-II onset in Sr^{2+}-activated eggs expressing or not human-PLCζ. The gray bars indicate average values. *, $p < 0.05$; Welch's t test. **b,** A graph showing the spindle rotation angle (magenta) and relative intensity of cytoplasmic Ca^{2+} levels (green) in representative Sr^{2+}-activated eggs expressing human-PLCζ. **c,** Heat map showing the normalized angular velocity (Δt = 1 min) of spindle rotation for several minutes before and after the Ca^{2+} transient in human-PLCζ expressing Sr^{2+}-activated eggs (48 peaks, 11 eggs). The timing of the Ca^{2+} transient is enclosed by a black square. **d,** Schematic of thapsigargin treatment for Ana-II eggs during live observation. **e,** Graph showing the spindle rotation angle (magenta) and relative intensity of cytoplasmic Ca^{2+} levels (green) in a representative thapsigargin-treated egg. Orange bars indicate the time of thapsigargin addition.

Fig.4 Cytoplasmic streaming inverts immediately after Ca^{2+} levels peak

a,d, Representative images showing chromosomes (magenta) and cytoplasmic Ca^{2+} levels (green) in a Sr^{2+}-activated egg **a**, or a Sr^{2+}-activated egg treated with 0.08 μg/mL nocodazole **d** at a time point before and immediately after the Ca^{2+} transient, merged with bright field (top panels).

Colored heat maps of vectors indicate the direction and velocity of cytoplasmic streaming analyzed using PIV as v-component (bottom panels). The numbers above the top panels indicate the time after Ana-II onset **a**, or Sr^{2+}-activation **d** (min). **b,e,** Graphs show the velocity of cytoplasmic streaming (blue) and relative intensity of cytoplasmic Ca^{2+} levels (green) in the eggs shown in **a** and **d**, respectively. The velocity of cytoplasmic streaming was analyzed within the orange frames in the upper panels of **a** and **d**. **c,f,** Heat maps showing the normalized velocity of cytoplasmic streaming for several minutes before and after the Ca^{2+} transient in Sr^{2+}-activated eggs (34 peaks, 11 eggs) **c**, or in Sr^{2+}-activated eggs treated with 0.08 μg/mL nocodazole (25 peaks, 6 eggs) **f**. The timing of the Ca^{2+} transient is enclosed by a black square.

Fig.5 Ca^{2+} oscillations ensure the extrusion of a small-sized PB2

a, Schematic showing the quantification of the spindle position and distance (*d*) between the midpoint of the spindle and centroid of the egg. **b,** Representative time-lapse images showing the spindle position of a Sr^{2+}-activated egg expressing mRFP1-tagged histone H2B (magenta). **c,** Graph showing the spindle position (purple) and mean velocity of cytoplasmic streaming (blue) for 30 min after Ana-II onset of an egg shown in **b**. **d,** Representative time-lapse images of a Sr^{2+}-activated egg with spindle detachment from the plasma membrane during early Ana-II. **e,** Graph showing the spindle position (purple) and mean velocity of cytoplasmic streaming (blue) for 40 min after Ana-II onset of an egg shown in **d**. **f,** Representative images show eggs at five hours of culturing after activation with Sr^{2+} (left), 7% ethanol (middle), and Sr^{2+} followed by thaprigargin treatment (right). White arrows indicate eggs with large PB2. **g,** Ratio of activated eggs with large and no PB2 under each activation condition. The numbers in the bars indicate the number of activated eggs in each category. n: number of activated eggs observed in each experiment. **h,** Model of the mechanism that ensures subcortical localization of the Ana-II rotating spindle.

Fig.6 Ca^{2+}-induced cytoplasmic streaming is oriented toward both parental chromosomes

Representative images showing chromosomes (magenta) and cytoplasmic Ca^{2+} levels (green) in an IVF egg at a time point before and immediately after the Ca^{2+} transient merged with a bright field (top panels). Vector maps indicating the direction and velocity of cytoplasmic streaming analyzed using PIV (bottom panels). Black arrows indicate the positions of sperm chromosomes. Numbers above the top panels indicate the time after the onset of Ana-II.

Fig.7 Direction of inverted cytoplasmic streaming is determined by spatial-asymmetric contractions of cortical actomyosin

a, Graph showing the velocity of cytoplasmic streaming (blue) and relative cytoplasmic Ca^{2+} levels (green) in a blebbistatin-treated Ana-II egg. A black arrowhead indicates the time of

blebbistatin addition. **b,** Changes in inward (yellow) and outward (blue) cytoplasmic streaming at 30 min after blebbistatin treatment. The gray bars indicate average values. **, $p < 0.01$; Mann-Whitney test. **c,** Schematics showing the area where F-actin fluorescence intensity and plasma membrane dynamics were measured. **d,** Kymographs showing the plasma membrane dynamics of the actin cap region (region #1 in **c**) (top) and the cortical region (region #2 in **c**) (middle), and the graph showing the relative F-actin fluorescence intensity in the three cortical regions (region #2, 3, 4 in **c**) (bottom) of a representative egg. The timescales of the kymographs and graphs were consistent. **e,** Heat maps showing the normalized velocity of cytoplasmic streaming (top) and normalized F-actin fluorescence intensity in three cortical regions (region #2, 3, 4 in **c**) (middle) and the cytoplasmic region (region #5 in **c**) (bottom) in activated eggs before and after cytoplasmic streaming inversion. The minute zero indicates the timing of cytoplasmic streaming inversion (black squares). **f,** Top, representative immunofluorescent images of F-actin (magenta) and pMLC (green) in Sr^{2+}-activated eggs with (top panels) and without (middle panels) cortical pMLC signals. Bottom, graphs show the fluorescence intensity profiles of F-actin and pMLC along the dashed white lines in the upper panels. **g,** Representative immunofluorescent images of F-actin and pMLC in Sr^{2+}-activated Ana-II eggs. Asterisks indicate eggs with cortical pMLC (top panel). The bottom graph shows cortical F-actin signal ratios. The gray bars indicate average values. ****, $p < 0.0001$; Mann-Whitney test. **h,** Model of Ca^{2+}-driven, chromosome-directed cytoplasmic flow.

Methods

Mice

The mouse strains used in this study were purchased from Charles River Laboratories (ICR mice) and CLEA Japan (female BALB/cA and male C57BL/6J mice). ICR mice were used for egg collection. Female BALB/cA and male C57BL/6J mice were cross-bred to obtain BALB/cA × C57BL/6L F1 (CB6F1) mice, which were then used for sperm collection. All mice used in this study were 8–24-week-old. The animal experiments were approved by the Animal Experimentation Committee of the Graduate School of Arts and Sciences, The University of Tokyo (approval no. 26-29) and performed following the guidelines for animal use issued by the Committee of Animal Experiments at The University of Tokyo.

Egg and sperm collection

Female mice (8–16-week-old) were superovulated by intraperitoneal injection of 5 IU of pregnant mare serum gonadotropin (ZENOAQ) for 48 h and 5 IU of human chronic gonadotropin (Kyoritsu Seiyaku) for 18–20 h prior to egg collection. Egg-cumulus complexes were collected in an M2 medium (M7167, Sigma-Aldrich) containing 100 μg/mL hyaluronidase to remove cumulus cells. Denuded Meta-II eggs were cultured in M16 medium (M7292, Sigma-Aldrich) covered with liquid paraffin (Specially Prepared Reagent, Nacalai tesque) at 37°C under 5% CO_2 until mRNA injection, followed by parthenogenic activation or insemination. Spermatozoa isolated from the cauda epididymis were precultured in HTF medium (ARK Resource) covered with liquid paraffin for at least 1 h at 37°C under 5% CO_2 before being used for insemination.

Egg activation

For Sr^{2+} activation, we used the Sr^{2+}-induced method [40]. Meta-II eggs were placed in M16 medium supplemented with 5 mM $SrCl_2$ and 5 mM EGTA and cultured at 37°C. For ethanol activation, Meta-II eggs were placed in M2 medium supplemented with 7% ethanol for 4.5 min at 25°C followed by washout and culture in M16 at 37°C. To induce high-frequency Ca^{2+} oscillations, Meta-II eggs microinjected with mRNA of human-PLCζ were inculcated for 30 min and then placed in M16 medium supplemented with 2.5 mM $SrCl_2$ and 2.5 mM EGTA at 37°C.

mRNA preparation and microinjection

mRNA was synthesized in vitro with linearized template plasmids using the RiboMax Large Scale RNA Production System-T7 (Promega) supplemented with the Ribo m^7G Cap Analog (Promega), as described previously[41]. Template plasmids for human-PLCζ were constructed using cDNA from a pcDNA-flag-human-PLCζ-AID-EGFP-polyA. The mRNA used for

474 microinjection were mRFP1-tagged histone H2B at 50 ng/μL, EGFP-α-tubulin at 200 ng/μL,
475 EGFP-UtrCH at 100 to 400 ng/μL, and human-PLCζ at 10 ng/μL. A minimal amount
476 (picoliters) of mRNA was microinjected into Meta-II eggs using a piezo-driven
477 micromanipulator (Prime Tech) and cultured for at least 3.5 h before being subjected to live
478 imaging.
479
480 **Live imaging**
481 Confocal images were collected with a microscope (IX71; OLYMPUS) equipped with a spinning
482 disk confocal system (CSU10; Yokogawa), 60x/1.30 Sil or 20x/0.85 NA oil objective lens
483 (OLYMPUS), and a CCD camera (iXon DU897E-CSO-#BV; ANDOR) controlled by Metamorph
484 (Universal Imaging). To observe spindle dynamics with a 60x/1.30 Sil objective lens, confocal
485 images were collected as z-stacks at 1-μm intervals (number of optical z-stacks:16) every minute.
486 To observe multiple eggs with a 20x/0.85 NA oil lens, confocal images were collected as z-stacks
487 at 5-μm intervals (number of optical z-stacks: 16) every minute.
488
489 **Live imaging of IVF eggs**
490 Removing cumulus cells causes the stiffness of the zona pellucida and prevents sperm from
491 passing through it. Therefore, after the microinjection of mRNA, a hole was made in the zona
492 pellucida some distance from the Meta-II spindle using a piezo-driven pipette for sperm entry
493 through the zona pellucida, as described previously[39]. Meta-II eggs were immobilized by
494 suctioning the position opposite the spindle with a holding pipette. Sperm cells separated using
495 the swim-up method were placed into the HFT medium so that the sperm concentration was 2.0
496 × 10^6/mL and were then cultured at 37℃ under 5% CO_2. For the live imaging of IVF eggs, we
497 prepared two adjacent 3-μL drops of M16 medium on a Φ3.5-cm glass-bottom dish, which was
498 covered with liquid paraffin. After adding the mRNA-microinjected eggs with the hole in the zona
499 pellucida and a few μl of 2.0 × 10^6/mL sperm to each medium drop, respectively, a glass-bottom
500 dish was placed in a stage-top incubator at 37℃ under 5% CO_2. After immobilizing the
501 orientation-adjusted Meta-II eggs using a holding pipette, insemination was performed by
502 connecting two drops using a glass needle.
503
504 **Live imaging of parthenogenetic-activated eggs**
505 mRNA-microinjected Meta-II eggs were washed in Sr^{2+} activation medium and transferred to 3
506 μL of Sr^{2+} activation medium covered with liquid paraffin on a glass-bottom dish. The orientation
507 of the Meta-II eggs was adjusted by mouth pipetting so that the Meta-II spindle was in the
508 equatorial plane of the eggs, with its axis parallel to the focal plane. A glass-bottom dish was then
509 placed in the stage-top incubator at 37℃ under 5% CO_2.

Monitoring the Ca^{2+} oscillation

To monitor the cytoplasmic Ca^{2+}, Meta-II eggs were microinjected with a few picotiters of 1 mg/mL of the Ca^{2+}-sensitive fluorescent dye, Cal520®-Dextran Conjugate *MW 3,000* or Cal-590™-Dextran Conjugate *MW 3,000* (AAT Bioquest), along with mRNAs for the expression of the protein(s) of interest, followed by culturing for 4 hours until the start of live imaging.

Drug treatment under live observation

Medium drops containing the drugs dissolved in DMSO were prepared as previously reported [28]. For the thapsigargin treatment assay, two Sr^{2+} activation medium drops, one containing 10 or 20μm thapsigargin and one without thapsigargin were placed close to each other on a glass-bottom dish and covered with 4 ml liquid paraffin followed by incubation at 37℃ under 5% CO_2 for 30 to 60 min before live imaging. Eggs were placed in the thapsigargin-free medium drop and the glass-bottom dish was placed in a stage-top incubator at 37℃ under 5% CO_2. After immobilizing the orientation-adjusted eggs using a holding pipette equipped on the stage of a confocal microscope, the two drops were connected using a glass needle–5–10 min after Ana-II onset. Blebbistatin was applied 10 min after Ana-II onset to a final concentration of 100 μM, using the same method as in the thapsigargin treatment assay.

Immunostaining

Eggs were placed in acidic Tyrode's solution to remove their zona pellucida, followed by washout with 0.5% polyvinyl pyrrolidone/PBS and fixation in 4% paraformaldehyde for 30 min at 25℃. Fixed samples were permeabilized with 0.1% Triton-X100/PBS for 15 min at 25℃ and then placed in a blocking solution (PBS containing 3% BSA and 0.1% Tween20) for 2 hours. After blocking, samples were incubated with the primary antibody, rabbit anti-phospho-myosin light chain 2 (Ser19) (pMLC) (1:100, Cell Signaling Technology #3671), for 2 hours, followed by three washes for 20 min. The samples were then incubated in the solution containing Alexa Fluor 488-conjugated goat anti-rabbit (1:500, A-11034, Invitrogen), rhodamine phalloidin (Invitrogen), and Hoechst 33342 dye (10 μg/mL, H-1399, Thermo Fisher Scientific) for 45 min, followed by three washes for 20 min. Z-stack images were collected at 1-μm intervals (number of optical z-stacks: 90) to visualize the entire eggs using a fluorescence microscope (IX70; OLYMPUS) equipped with 60x/1.30 NA Sil or 20x/0.85 NA oil objective lens (OLIMPUS) and a cold CCD camera (CoolSNAP HQ; Roper Scientific) that was controlled using Delta Vision SoftWorx (Applied Precision). The Z-stack images were then deconvoluted.

Image analysis

To quantify the spindle rotation angle, the centroid of each separated chromosome (10 min after Ana-II onset before the beginning of spindle rotation), the egg, and the spindle midpoint were tracked by image processing using ImageJ. For the chromosome centroid, fluorescence images of the chromosomes (H2B-mRFP1) were smoothed with a median filter (radius = 2) and binarized using a threshold (Yen algorithm). For the egg centroid, the cytoplasmic fluorescence images of Cal-520-dextran or EGFP-α-tubulin or H2B-mRFP1 were smoothed with a median filter (radius = 10), then binarized using a threshold (Otsu algorithm). The centroid coordinates of the binarized images, defined as the x-y coordinates, were calculated using ImageJ. The spindle midpoint was defined as the midpoint between the centroids of the separated chromosome signals. The spindle rotation angle was quantified as the angle between the line connecting the centroids of the separated chromosome signals and the line connecting the egg centroid and spindle midpoint. The coordinates of the chromosome centroids at n min after Ana-II onset were defined as A (a_n, b_n) for the chromosomes eventually extruded as PB2 and A' (c_n, d_n) for the chromosomes remaining in the eggs. The coordinates of the spindle midpoint and egg centroid n min after Ana-II onset were defined as B (e_n, f_n) and B' (g_n, h_n), respectively. The rotation angle is given by

$$\cos\theta = \frac{(c_n - a_n) \times (g_n - e_n) + (d_n - b_n) \times (h_n - f_n)}{\sqrt{(c_n - a_n)^2 + (d_n - b_n)^2} \times \sqrt{(g_n - e_n)^2 + (h_n - f_n)^2}} \quad (n \geqq 10)$$

Conversion from radians to angles is given by

$$\alpha^\circ = \frac{180}{\pi} \times \theta$$

where α° is the rotation angle. The angles were normalized by subtracting all angles from the initial angle to calculate the rotation angle from the initial spindle position. To quantify normalized changes in the rotation angle, the angular velocity (Δt = 1 min) a few minutes before and after the Ca^{2+} transient was divided by the absolute maximum angular velocity for the same period. All Ca^{2+} transients were maintained for 30 min during spindle rotation.

To quantify the spindle position within the egg, the distance (d) between the spindle midpoint and egg centroid was calculated. The coordinates of both the spindle midpoint and egg centroid were obtained using the same method as that used to quantify the spindle rotation angle.

Ca^{2+} oscillations were analyzed using the fluorescence signals of Cal-520-dextran. To measure the relative intensity of Cal-520-dextran, its cytoplasmic fluorescence images were smoothed using a median filter (radius = 10) and binarized using a threshold (Otsu algorithm). After defining a region of interest (ROI) using the binarized images of Cal-520-dextran, its mean fluorescence signals within the ROIs were measured. To calculate the relative intensity of cytoplasmic Ca^{2+},

Cal-520-dextran signals at each time point were divided by the minimum intensity for 30 min during spindle rotation.

The cortical F-actin intensity in live eggs was measured using EGFP-UtrCH fluorescence signals. A wide range of five pixels of cortical F-actin fluorescence signal was measured as cortical F-actin intensity. To obtain a width of 5 pixels, cytoplasmic fluorescence signals of histone H2B-mRFP1 were smoothed with a median filter (radius = 10) and binarized using a threshold (Otsu algorithm). Second, two binarized images were eroded or dilated so that the difference between the larger and smaller regions was 5 pixels, and ROIs were defined in each image, followed by the measurement of the mean fluorescence intensity of EGFP-UtrCH within the ROIs. Third, the mean fluorescence intensity of the dilated ROI was subtracted from that of the eroded ROI. Three cortical regions were selected for the analysis of cortical F-actin intensity. To calculate the relative intensity of cortical F-actin, the EGFP-UtrCH intensity at each time point was divided by the minimum intensity during 30 min of spindle rotation. For normalization, the relative intensity of cortical F-actin a few minutes before and after the cytoplasmic streaming inversion was divided by the absolute maximum intensity of cortical F-actin for the same period.

To validate the cortical myosin II activity in fixed eggs, the fluorescence intensity of pMLC was measured using the plot profile (line width: 20 pixels) in ImageJ. The line for the plot profile was drawn across the center of the egg to avoid the actin cap regions.

To validate the fluorescence intensity of cortical F-actin in the fixed eggs, the average of the two peak values of cortical F-actin intensity, measured using the plot profile (line width: 20 pixels), was calculated after subtracting the background intensity. Ratios of cortical F-actin intensity were obtained by dividing the average intensity of cortical F-actin in eggs with cortical pMLC signals by that in eggs without cortical pMLC signals.

The fluorescence intensities of pMLC and F-actin in the cortical region were analyzed using the fluorescence signals of maximum intensity z-projections (ten z-slices) around the egg equatorial plane.

All heat maps of the normalized values for each image analysis were generated using GraphPad Prism9 software.

PIV analysis

To analyze cytoplasmic streaming, cytoplasmic particle dynamics were tracked using the PIVlab package[42]. Fluorescent time-lapse images merged with a bright field were used to simultaneously analyze cytoplasmic streaming with spindle rotation and Ca^{2+} oscillations. Because the egg in the time-lapse images moved slightly in the x-y plane, the StackReg plugin written for ImageJ was used to stabilize the position of the eggs before PIV analysis. The non-egg area was masked to exclude vectors outside the egg. We used the following parameters for PIV analysis, similar to

those previously described[19,20]: CLAHE window size: 100 pixels, high-pass kernel size: 10 pixels, interrogation area of pass 1: 70 pixels, interrogation area of pass 2: 35 pixels, sub-pixel estimator: Gauss 2x3-point, correlation robustness: standard. The analyzed vector maps were adjusted and smoothed using vector validation and modification functions, respectively. For display purposes, the velocity magnitude of cytoplasmic streaming in the y-axis direction of the x-y plane (the axis perpendicular to the spindle) was colored using the v-component of the display function. The blue color indicates a positive value of streaming toward the spindle, and the yellow color indicates a negative value of streaming opposite the spindle. After obtaining vector maps of consecutive frames, the mean value of the vectors within a specific square area below the spindle was calculated as the velocity and direction of cytoplasmic streaming, as shown in Fig 2**a,d**. To quantify the normalized velocity of cytoplasmic streaming, the velocity of cytoplasmic streaming minutes before and after the Ca^{2+} transient was divided by the absolute maximum velocity during the same period. All Ca^{2+} transients were selected for 30 min during spindle rotation. Heat maps of normalized cytoplasmic streaming were created using the GraphPad Prism9 software.

Quantifications and statistical analysis

Statistical analyses were performed using R or GraphPad Prism9. First, the normality of the data was checked using the Shapiro–Wilk test. The data shown in Extended Data Fig. **3a** were parametric and tested using Welch's t-test. The data in Fig. **7b,g** are non-parametric and were tested using the Mann–Whitney *U* test. For representative images, experiments were performed at least thrice. All experiments involving eggs were performed at least two or more times, where n denotes the number of eggs.

Data availability

The data that support the finding of this study are available from the authors upon request.

641 **Method references**

642 40. Kishigami, S. & Wakayama, T. Efficient strontium-induced activation of mouse oocytes
643 in standard culture media by chelating calcium. *J. Reprod. Dev.* **53**, 1207–1215 (2007).
644 41. Yamagata, K. *et al.* Noninvasive visualization of molecular events in the mammalian
645 zygote. *Genesis* **43**, 71–79 (2005).
646 42. Thielicke, W. & Stamhuis, E. J. PIVlab – Towards User-friendly, Affordable and
647 Accurate Digital Particle Image Velocimetry in MATLAB. *J. Open Res. Softw.* **2**,
648 (2014).
649

Acknowledgements

We thank Tomo Kondo (The University of Tokyo) for advice on setting up a holing pipette, Kazuo Yamagata (Kindai University) for advice on the time-lapse imaging of mouse eggs, Atsuo Ogura (RIKEN BRC) and Junya Ito (Azabu University) for the human-PLCζ constructs, Hiroshi Kimura (Tokyo Institute of Technology) for the mRFP1-tagged histone H2B constructs, Bill Bement (University of Wisconsin-Madison) for the EGFP-UtrCH constructs. The research was supported by the Japan Society for the Promotion of Science KAKENHI (grant numbers 21J11440 to T.T.; 20H03250, 20H05356, 22H04664 and 23H02485 to M.O.).

Author contributions

T.T. and M.O designed the research. T.T. performed all experiments and data analysis. T.T. and M.O. wrote the manuscript.

Competing interests

The authors declare no competing interests.

Extended Data Figure legends

Extended Data Fig.1 Transient inversions in the direction of spindle rotation is dependent on Ca^{2+} oscillations.

a,b,c, Graphs showing the spindle rotation angle (magenta) and relative intensity of cytoplasmic Ca^{2+} levels (green) (top panels), and the angular velocity of (Δt = 1 min) of spindle rotation and changes in the relative intensity of cytoplasmic Ca^{2+} for 30 min during spindle rotation (bottom panels) in four representative IVF **a**, or Sr^{2+}-activated **b,** or human-PLCζ expressing Sr^{2+}-activated **c** eggs. **d,** Graphs showing the spindle rotation angle (magenta) and relative intensity of cytoplasmic Ca^{2+} levels (green) in three representative thapsigargin-treated eggs. Orange bars indicate the time of thapsigargin addition.

Extended Data Fig.2 Inversion of cytoplasmic streaming immediately after the Ca^{2+} transient cause a reversal of spindle rotation.

a,c, Graphs showing the velocity of cytoplasmic streaming (blue) and relative intensity of cytoplasmic Ca^{2+} levels (green) in three representative Sr^{2+}-activated eggs **a**, or Sr^{2+}-activated eggs treated with 0.08 μg/mL nocodazole **c**. **b,** Graphs showing the velocity of cytoplasmic streaming (blue) and angular velocity of spindle rotation (Δt = 1 min) (magenta) in four representative Sr^{2+}-activated eggs.

Extended Data Fig.3 Inversed cytoplasmic streaming is oriented towards both maternal and paternal chromosomes.

Representative images showing chromosomes (magenta) and cytoplasmic Ca^{2+} levels (green) in an IVF egg at a time point before and immediately after the Ca^{2+} transient merged with a bright field (top panels). Vector maps indicating the direction and velocity of cytoplasmic streaming analyzed using PIV (bottom panels). Black arrows indicate the positions of sperm chromosomes. Numbers above the top panels indicate the time after the onset of Ana-II.

Extended Data Fig.4 Inhibition of myosin II activity decrease the velocity of cytoplasmic streaming but not compromise Ca^{2+} oscillations.

Graphs showing the velocity of cytoplasmic streaming (blue) and relative cytoplasmic Ca^{2+} levels (green) in three representative blebbistatin-treated Ana-II eggs. Black arrowheads indicate the time of blebbistatin addition.

Extended Data Fig.5 MLC phosphorylation at the cortex in Sr^{2+} activated eggs.

a,b, Left, three representative fluorescent images of F-actin and pMLC in Sr^{2+} activated eggs with **a** or without **b** cortical pMLC singals. Right, graphs show the fluorescence intensity

profiles of F-actin and pMLC along the dashed white lines in the left panels. **c,** Left, three representative fluorescent images of F-actin and pMLC in 7% EtOH activated eggs. Right, graphs show the fluorescence intensity profiles of F-actin and pMLC along the dashed white lines in the left panels. White ellipses indicate the Ana-II spindle.

Supplementary Videos

Supplementary Video 1

Dynamics of the Spindle and Chromosomes in an IVF Egg

Time-lapse observation of an IVF egg injected with mRFP1-tagged histone H2B (to label chromosomes, magenta) and EGFP-α-tubulin (to label spindle, green). Video of chromosomes, merged with bright field (left), and chromosomes and the spindle (right). The number in videos indicate the time after Ana-II onset (hr :min).

Supplementary Video 2

Dynamics of the chromosomes and Ca^{2+} oscillations in an IVF egg, or a Sr^{2+}-activated egg

Time-lapse observation of an IVF (top panels), or a Sr^{2+}-activated egg (bottom panels) injected with mRFP1-tagged histone H2B (to label chromosomes, magenta) and Cal520-dextran (to label cytoplasmic Ca^{2+}, green). Video of chromosomes, merged with bright filed (left), and chromosomes and cytoplasmic Ca^{2+} (right). The number in videos indicate the time after Ana-II onset (hr :min).

Supplementary Video 3

Periodical inversion of cytoplasmic streaming in a Sr^{2+} activated egg

Time-lapse observation of a Sr^{2+} activated egg injected with mRFP1-tagged histone H2B (to label chromosomes, magenta) and Cal520-dextran (to label cytoplasmic Ca^{2+}, green), merged with bright field (left). Colored heat maps of vectors indicate the direction and velocity of cytoplasmic streaming analyzed using PIV as v-component (right). The number in videos indicate the time after Ana-II onset (hr :min).

Supplementary Video 4

Periodical inversion of cytoplasmic streaming in a Sr^{2+} activated egg in the absence of spindle rotation

Time-lapse observation of a Sr^{2+} activated egg injected with mRFP1-tagged histone H2B (to label chromosomes, magenta) and Cal520-dextran (to label cytoplasmic Ca^{2+}, green), merged with bright field (left). Colored heat maps of vectors indicate the direction and velocity of cytoplasmic streaming analyzed using PIV as v-component (right). The number in videos indicate the time after Sr^{2+}-activation (hr :min).

Supplementary Video 5

Suppression of Ca^{2+} oscillations in a Sr^{2+} activated egg

Time-lapse observation of Sr^{2+} activated eggs injected with mRFP1-tagged histone H2B (to label

chromosomes, magenta) and Cal520-dextran (to label cytoplasmic Ca^{2+}, green). Video of chromosomes and cytoplasmic Ca^{2+} (left), and chromosomes, merged with bright filed (right). Top and bottom panels show representative images of the formation of the small-sized PB2 or the large-sized PB2, respectively. The number in videos indicate the time after Ana-II onset (hr :min).

Supplementary Video 6

Patterns of cytoplasmic streaming in an IVF Ana-II egg

Time-lapse observation of an IVF egg injected with mRFP1-tagged histone H2B (to label chromosomes, magenta) and Cal 520-dextran (to label cytoplasmic Ca^{2+}, green), merged with bright field (left). Vector maps indicate the direction and velocity of cytoplasmic streaming analyzed using PIV (right). The number in videos indicate the time after Ana-II onset (hr :min).

Supplementary Video 7

Decrease in the velocity of both inward and outward cytoplasmic streaming in a blebbistatin treated egg

Time-lapse observation of a Sr^{2+} activated egg injected with mRFP1-tagged histone H2B (to label chromosomes, green) and Cal 590-dextran (to label cytoplasmic Ca^{2+}, green) in the presence of blebbistatin, merged with bright field (left). Colored heat maps of vectors indicate the direction and velocity of cytoplasmic streaming analyzed using PIV as v-component (right). The number in videos indicate the time after Ana-II onset (hr :min).

Supplementary Video 8

Periodic changes in F-actin intensity in a Sr^{2+} activated egg

Time-lapse observation of a Sr^{2+} activated egg injected with mRFP1-tagged histone H2B (to label chromosomes, magenta) and EGFP-UtrCH (to label F-actin, green). The number in videos indicate the time after Ana-II onset (hr :min).

Fig.1

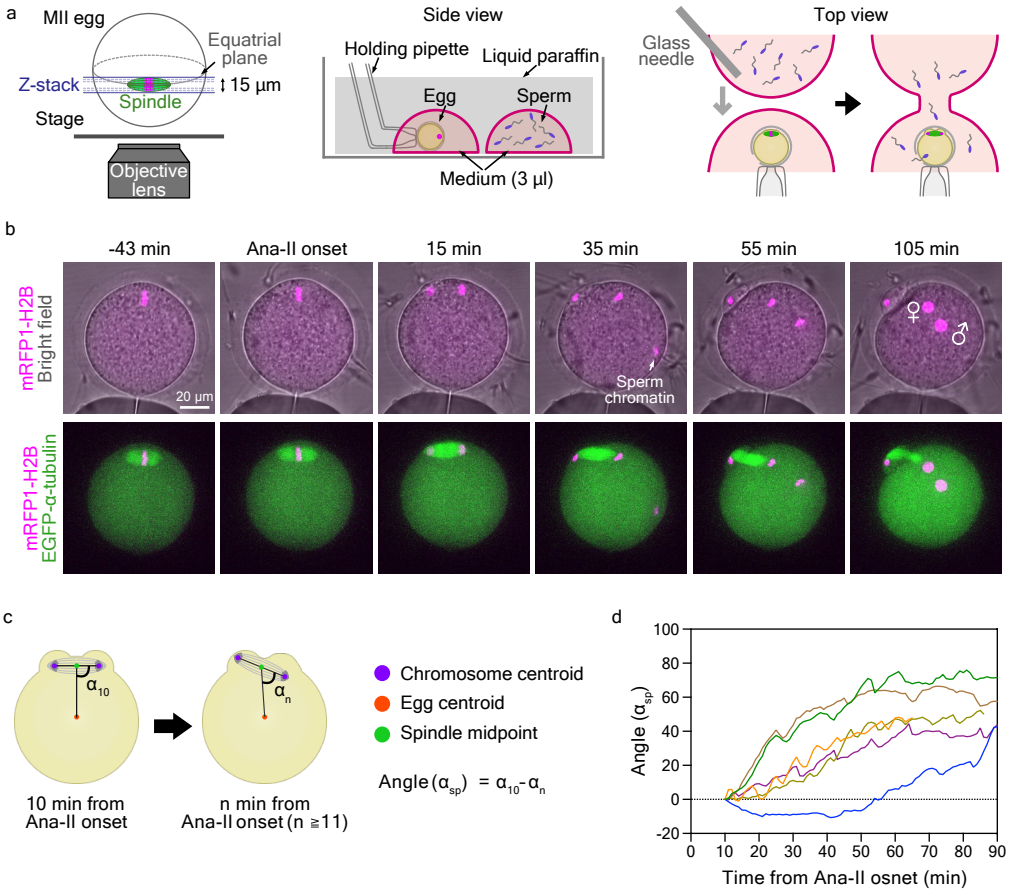

Fig.2

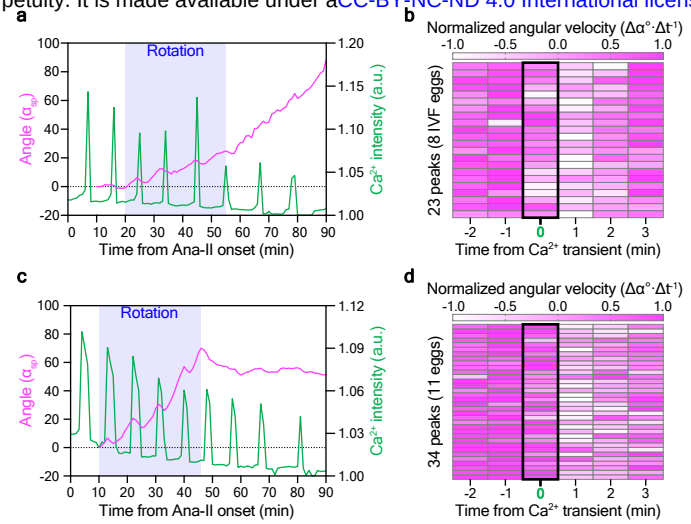

Fig.3

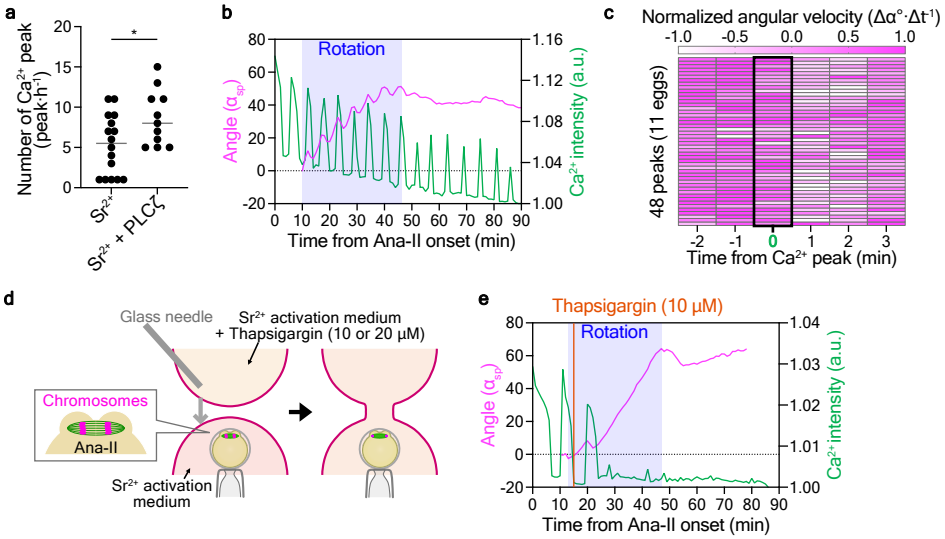

Fig.4

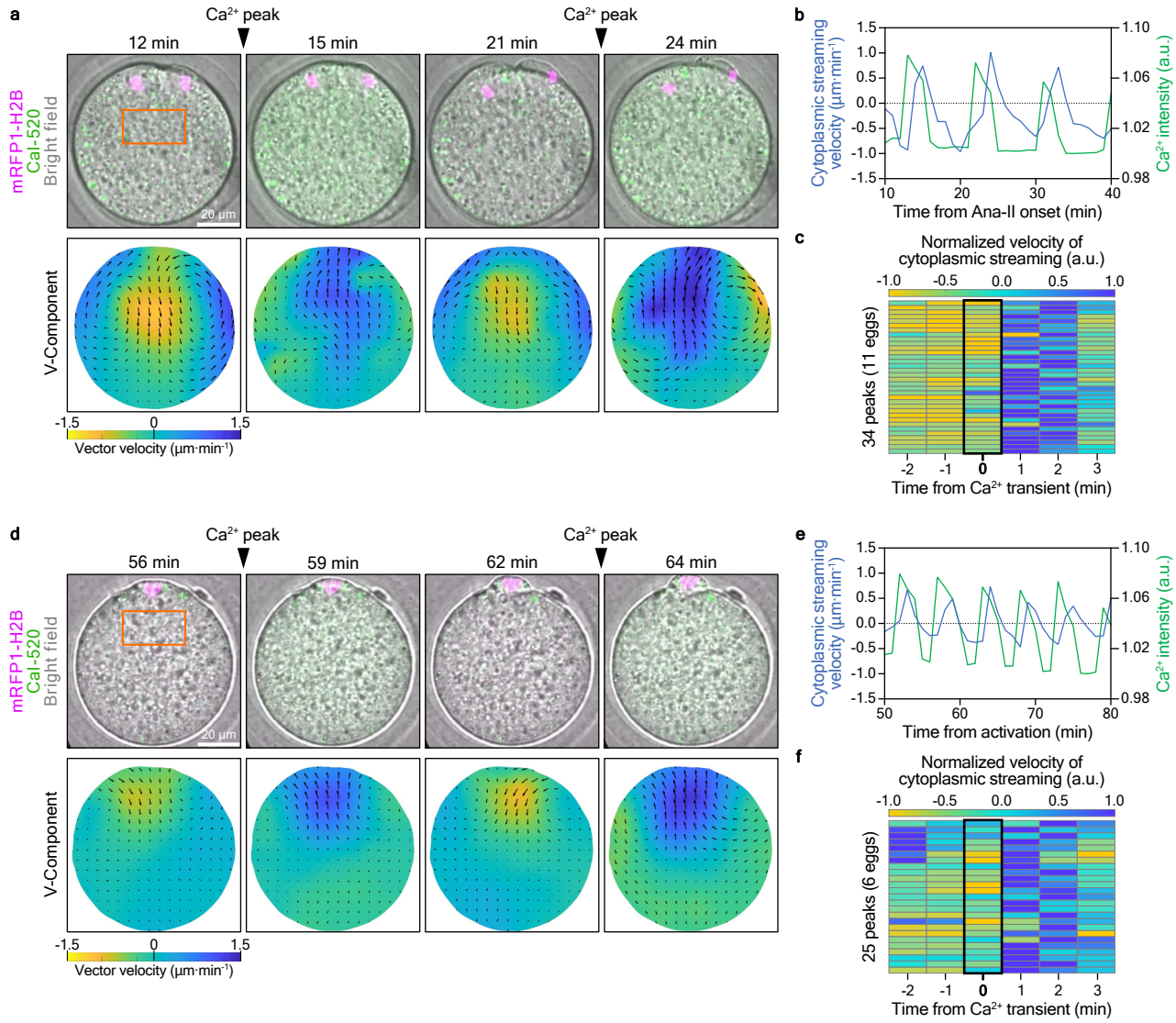

Fig.5

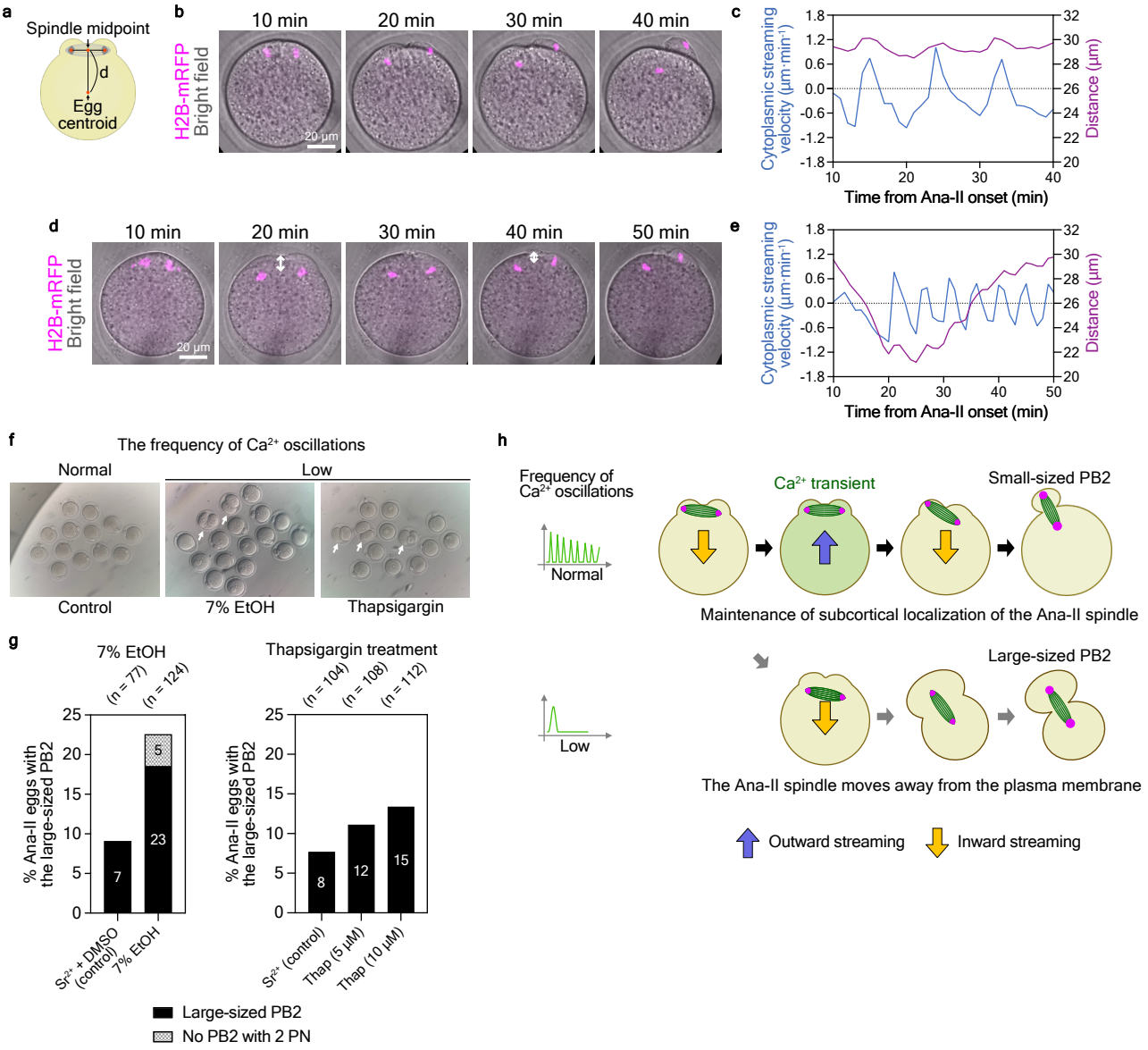

Fig.6

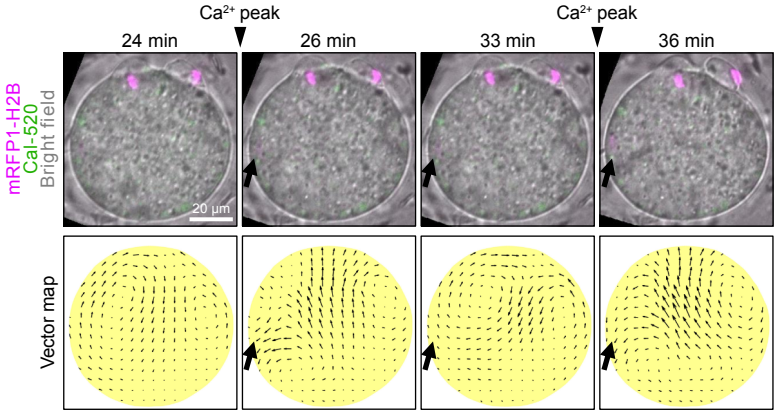

Fig.7

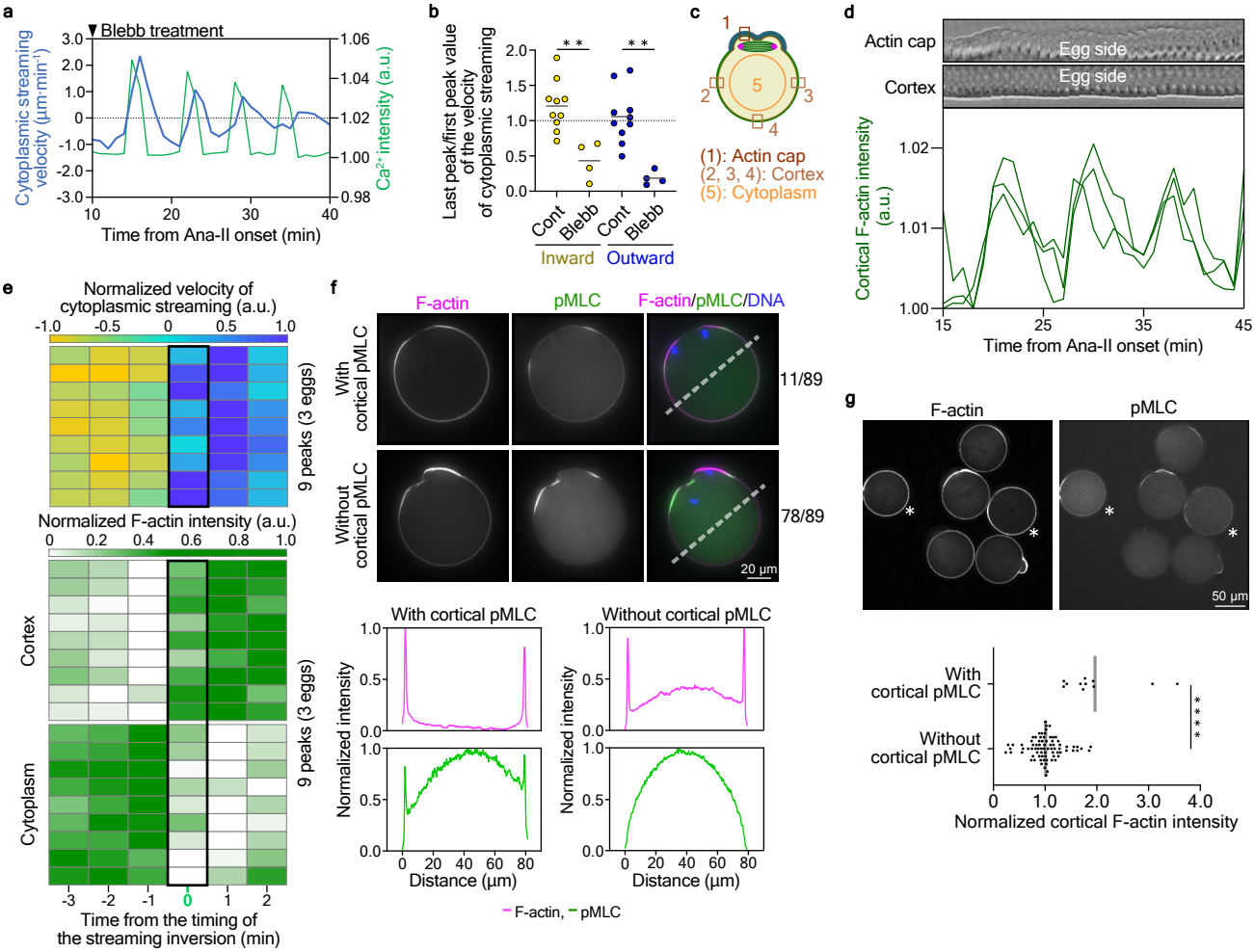

Extended data Fig.1

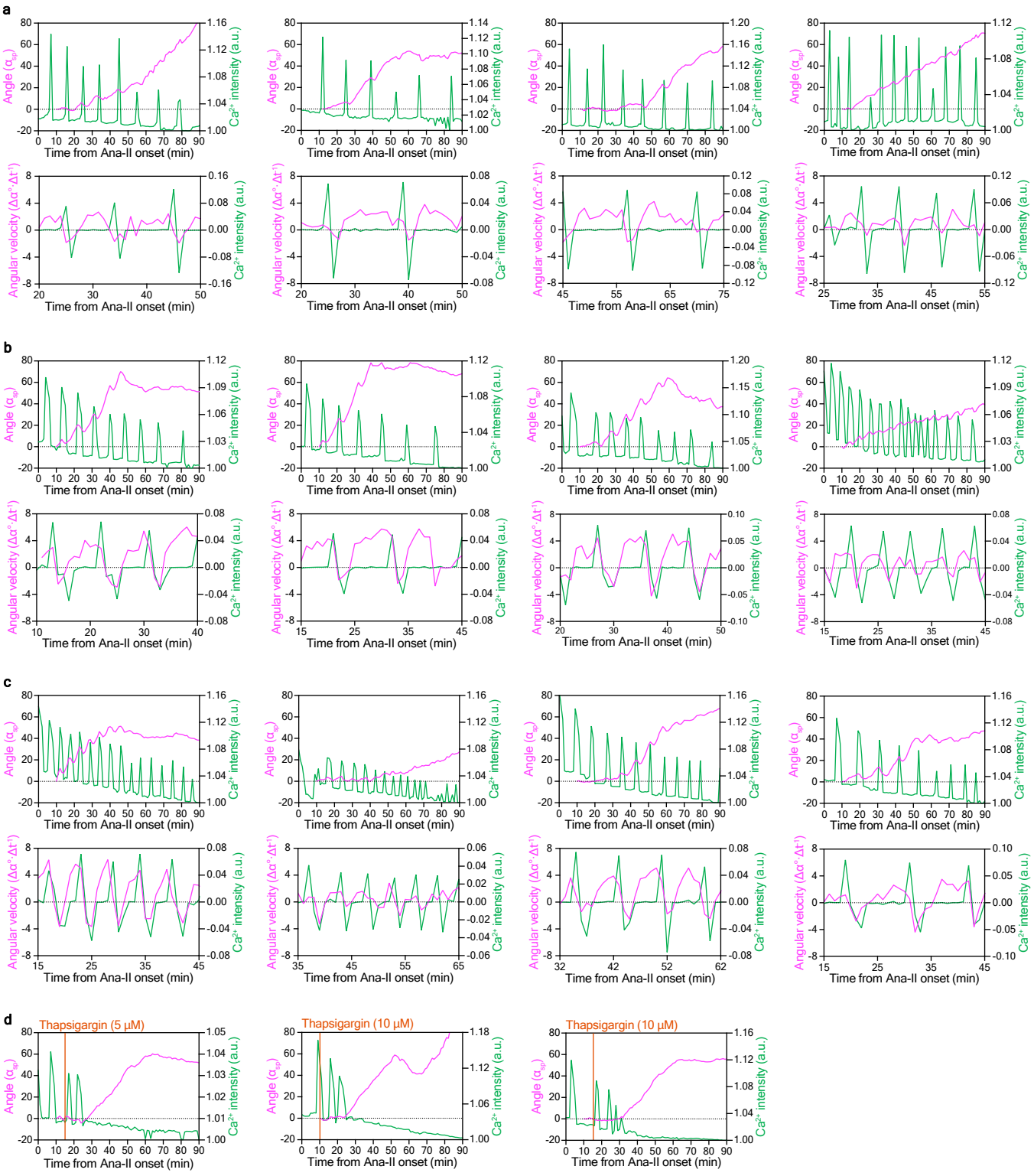

Extended data Fig.2

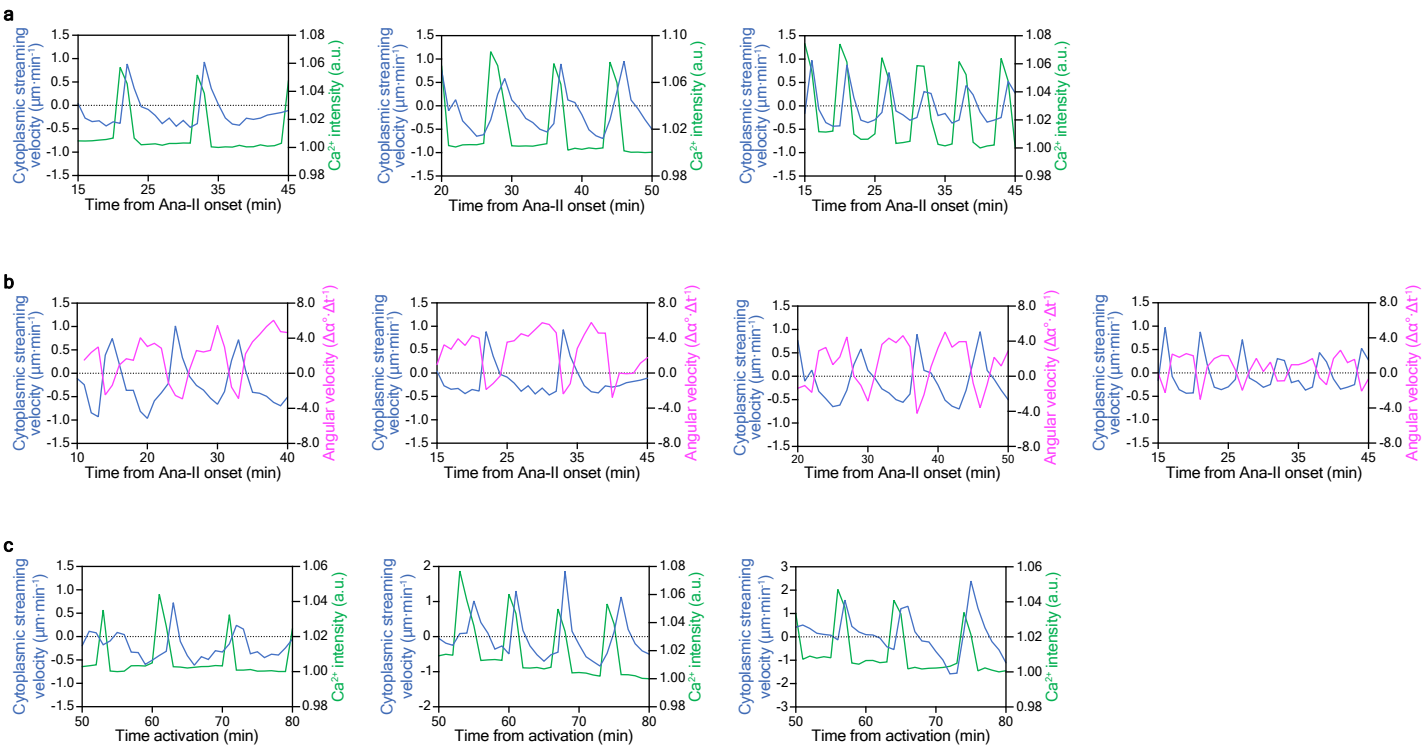

Extended data Fig.3

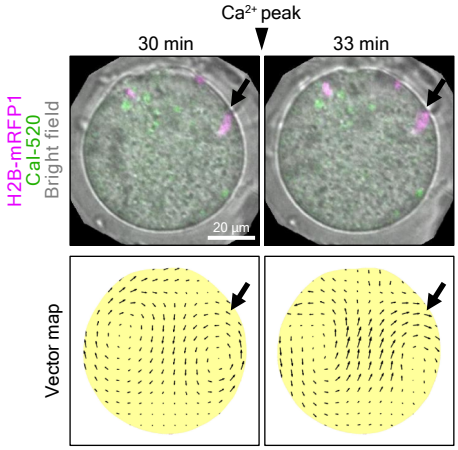

Extended data Fig.4

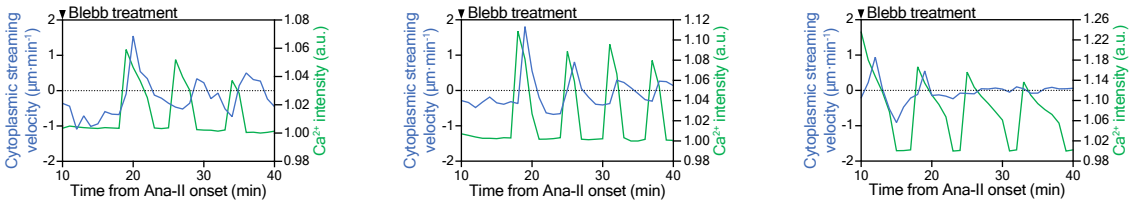

Extended data Fig.5